Modelling of Solid-State Fermentation over Wide Operational Range for Application in Process Optimization

Rafael F. Fonseca,[1,2]* Caio C. B. Melo,[2] Beatriz B. C. P. Sanches,[2] Victor Bertucci-Neto,[2] Cristiane S. Farinas[1,2] and Wu H. Kwong[1]

1. Graduate program of Chemical Engineering, Federal University of São Carlos, 13565-905, PO Box 676, São Carlos, SP, Brazil

2. Embrapa Instrumentação, Rua XV de Novembro 1452, 13560-970, São Carlos, SP, Brazil

The major drawbacks in large-scale solid-state fermentation processes are related to difficulty in controlling the medium temperature and moisture content, which are variables that directly affect microbial growth and product formation. Several mathematical models have been developed to describe these effects, although none has simultaneously considered distinct growth phases, growth restrictions caused by large temperature variations at several distinct moisture content conditions, and product formation pathways. In this manner, the objectives of this paper were to develop a mathematical model to represent the process under different operational conditions and a model-based optimization procedure to investigate the effects of varying temperature profiles to maximize a (hemi) cellulolytic enzyme production during cultivation of *Aspergillus niger* under solid state fermentation. The proposed model correlates fungal growth with the CO_2 production rates and with enzymatic production by the Luedeking-Piret function. It was developed with data acquired in a laboratory-scale column-type bioreactor in controlled conditions of aeration, temperature, and inlet air relative humidity. The developed model accurately predicted the respiration profile responses at all temperatures, under the most productive moisture content conditions. Incubation of the culture with the optimized temperature profile improved the enzymatic production, compared to the estimated optimum static temperature. These findings demonstrate the usefulness of this model for the optimization of larger-scale SSF processes.

Keywords: solid-state fermentation, mathematical modelling, parameter estimation, model-based optimization, (hemi) cellulolytic enzyme production

INTRODUCTION

Solid-state fermentation (SSF) involves cultivation of microorganisms, mostly fungi, in environments characterized by the absence or near-absence of free water. Solid wastes such as sugarcane bagasse, soybean bran, corn stover, and wheat straw can be used as growth substrates for microorganisms to produce enzymes and organic acids, among other products of industrial relevance.[1–4] However, the difficulties related to monitoring and controlling the temperature and moisture content of the medium are major limitations for industrial application of the SSF process, because these variables directly affect fungal growth and product formation.[5,6] As an example, in a packed-bed SSF bioreactor, the medium temperature can present variation up to 3 °C/cm,[7] although, if a forcefully-aerated bioreactor is used with these conditions, due to the evaporative cooling effect, the moisture content will vary along the associated substrate.[8] To mitigate the presented limitations, a kinetic study associated with a model development of a SSF process under several different operational conditions could help to improve overall process efficiency in larger-scale SSF due to enhanced controller actions.

The logistic equation is extensively used to describe biomass growth during SSF. Hamidi-Esfahani et al.[5] used it to model an *Aspergilus niger* cultivation at several different operational conditions. The biomass weight was determined by a glucosamine estimation method. The model parameters were expressed as a function of the temperature and of the initial moisture content. Subsequently, Hamidi-Esfahani et al.[9] developed a two-phase model using oxygen uptake rate to represent cellular growth, which was based in previous studies.[10,11] The growth was divided into an exponential phase, which was followed by a logistic equation that described the growth limits. No product formation was measured in either paper. Saithi et al.[12] investigated how the temperature and the moisture content affected microbial growth and product formation kinetics, and developed a process model to represent these effects under diverse fixed initial operational conditions. An association of a logistic equation with a Luedeking-Piret product formation was used to describe cellular growth using the accumulated CO_2 from cellular respiration to estimate it. The modelling indicated that the product formation was mainly growth-related. However, variations in temperature can also cause alterations in the microbial metabolic pathways,[13] such that under certain operational conditions, growth-associated product formation yields could change to non-growth-associated, which should also be taken into account during bioprocess development.[14]

Temperature variations that negatively impact the fungal growth during SSF cultivations were modelled by Dalsenter et al.,[15] who added a viability term to a logistic equation in order to describe the physiological state of the cells. The proposed model was validated using three distinct temperature profiles, showing that once the process temperature increased above the optimum for microbial growth, the cells would be irreversibly affected,

* *Author to whom correspondence may be addressed.*
E-mail address: rfrederico@gmail.com
Can. J. Chem. Eng. 96:1723–1734, 2018

DOI 10.1002/cjce.23088
Published online 30 November 2017 in Wiley Online Library (wileyonlinelibrary.com).

diminishing their growth capacity and consequently decreasing product formation.[15] None of the previous studies has simultaneously considered how the operational condition variations would affect product formation pathways and cause restrictions in the cellular physiological state. Given the importance of the temperature and moisture content on the microbial metabolic pathways, the development of models that are sensible to operational condition variations is interesting for the optimization of large-scale processes.

This work proposes a model that correlates fungal growth with the CO_2 production rates from the microbial respiration by *Aspergillus niger* under SSF.[12] The model also includes the effects of process temperature and substrate initial moisture content in the respiration profiles and correlates them to the xylanase and endoglucanase production using the Luedeking-Piret function.[14] The growth kinetics was described by a set of six logistic equations, divided into three separate growth phases. Growth parameters were estimated according to the CO_2 production rate during the cultivations, and product formation was determined by measuring the enzymatic activities during the process. In addition, a computational search routine was developed to find a varying temperature profile that could maximize enzymatic production by exploiting fungal growth and enzyme formation at different temperatures. The model was validated by experiments conducted in a column-type SSF bioreactor under controlled conditions of aeration, temperature, and inlet air relative humidity.[16] The search algorithm was based on a mixed nonlinear integer iterative programming algorithm and evolutionary techniques.[17] In this procedure, the temperature can change by a combination of -1 °C, 0 °C, or $+1$ °C per hour, within a fixed number of steps, which are simulated in the nonlinear model. At each new iteration, the first action of the best enzymatic production profile is recorded and subsequently, the search horizon is moved forward. This is repeated until the chosen process ending time is reached.

THEORETICAL BACKGROUND

The oxygen uptake rate can be used to describe fungal growth kinetics. As proposed by Hamidi-Esfahani et al.,[9] the model can correlate biomass growth with the oxygen uptake rate due to growth and cellular maintenance. The growth kinetic was separated in two phases, an exponential growth followed by a logistic law. In this study,[9] the experiments were carried out in a temperature controlled column-type bioreactor, with uncontrolled inlet air relative humidity. The idea of splitting the growth into two phases was previously employed by Ikasari and Mitchell,[11] where the model was developed to describe fast-acceleration/slow-deceleration growth profiles. The model can be described by Equations (1) and (2):

$$\frac{dX}{dt} = \begin{cases} \mu X, & t < t_a \\ \mu X\left(1 - \dfrac{X}{X_M}\right), & t \geq t_a \end{cases} \tag{1}$$

$$r_{O_2} = Y_{O_2X}\frac{dX}{dt} + mX \tag{2}$$

where X is the biomass content; r_{O_2} is the rate of O_2 consumption; Y_{O_2X} is the O_2 consumption yield related to cell growth; and m is related to cellular maintenance.

Another point of this work was how the process temperature variation affects the fungal growth and cellular physiological state. To this end, Dalsenter et al.[15] developed a cellular viability factor that limits the growth capacity when the microorganism is exposed to temperatures above its optimum growth temperature, as shown in Equations (3) and (4). Here, k_s and k_D are synthesis and denaturation coefficients, as a function of temperature, according to the Arrhenius equation; μ is the specific growth rate at the optimum temperature for growth; F is the cellular viability factor; X_M is the maximum possible biomass content; and X is the biomass content.

$$\frac{dF}{dt} = k_S F(1 - F) - k_D F \tag{3}$$

$$\frac{dX}{dt} = \mu X F\left(1 - \frac{X}{X_M}\right) \tag{4}$$

Saithi et al.[12] modelled the kinetics of growth and enzyme production under several distinct operational conditions, using a logistic equation to describe growth and the Luedeking-Piret equation to represent product formation, as shown in Equations (5) and (6). A cardinal temperature model with inflection was used to interpolate the growth and product formation parameters across the experimental temperature conditions. This approach provides a good fit for temperature, but does not take into account the influence of the moisture content. In Equation (6), the parameters α and β are the growth-related and non-growth-related product yields, respectively, P is the product of interest, and i is the i^{th} product evaluated. Diaz et al.[18] used the same modelling as Saithi et al.,[12] but included an inactivation term to the enzymatic activity, the term $-k_{D_i}P_i$ in Equation (6). This approach allowed them to calculate the maximum enzymatic production for several different processes, with distinct microorganisms and substrates involved.

$$\frac{dX}{dt} = \mu X\left(1 - \frac{X}{X_M}\right) \tag{5}$$

$$\frac{dP_i}{dt} = \alpha_i\frac{dX}{dt} + \beta_i X - k_{D_i}P_i \tag{6}$$

Another approach to describe the kinetics of cellular death or inactivation was described by Mitchell et al.,[6] using a set of two logistic equations representing the active cells and the total biomass produced, as shown in Equations (7) and (8). The main difference between this modelling approach and the one proposed by Dalsenter et al.[15] was that the population was divided into active and total cells. The main advantage of this approach was the use of a more accurate version of Equation (2) to express the respiration profile, described by Equation (9), where only active cells contribute to respiration gases production, otherwise CO_2 production or oxygen uptake would never cease in the process. This statement can also be valid to the other products of interest.

$$\frac{dX_a}{dt} = \mu X_a\left(1 - \frac{X_T}{X_M}\right) - k_d X_a \tag{7}$$

$$\frac{dX_T}{dt} = \mu X_a\left(1 - \frac{X_T}{X_M}\right) \tag{8}$$

$$r_{O_2} = Y_{O_2X}\frac{dX_T}{dt} + mX_a \tag{9}$$

EXPERIMENTAL PROCEDURES

Microorganism

The microorganism used in this study was a mutant strain of *Aspergillus niger* (*A. niger* 3T5B8) from the Embrapa Food Technology collection (Rio de Janeiro, Brazil). Stock cultures were stored at 4 °C on potato dextrose agar (PDA) slants. The cultures were revitalized and maintained on PDA slants at 32 °C for 5 days prior to inoculation.

Bioreactor Description

A column-type bioreactor with 20 mL of useful volume was used for the fermentations. This bioreactor presents two important characteristics for this study: 1) It is equipped with a forced aeration system, which will avoid oxygen limitation during microbial growth, 2) its dimensions assure that the external and the bulk medium temperature are virtually the same, which allows the study of different operational conditions similar to the ones observed in large-scale industrial bioreactors.[16,19,20] The inlet airflow and relative humidity were controlled at 20 mL/min and 80 %, respectively, which have been selected in previous studies.[16] These conditions were achieved using a proportional-integrative (PI) feedback controller to adjust the airflow ratio between two air flow lines, e.g. lines from a dryer and a humidifier devices, in order to keep both the relative humidity and airflow constant. The columns were kept in a water bath tank, whose temperature was controlled by a PI controller. A humidity sensor was installed inside an immersed column to measure the airflow relative humidity and the process temperature. A data acquisition device was used to sample, compute, and store all the measurements, as well as to manage the airflow and temperature actuators.

Solid-State Fermentation (SSF)

A previously washed and dried wheat bran 5 g mass was sterilized by autoclaving at 121 °C for 15 min for each inoculated column. After this procedure, the particles size varies in diameter from 0.5 to 2.0 mm. The initial substrate moisture content was adjusted using 1.8 mL of a 0.9 % (w/v) solution of ammonium sulphate in 0.1 mol/L HCl and subsequent addition of water to achieve the values established according to the experimental design (Table 1). The initial moisture content was calculated on a wet weight basis, using $M_C(\%) = W_m/(W_m + D_M)$, where W_m is the wet mass and D_M is the dry mass. In this sense, a $M_C = 50$ % indicates that the moisture mass is equal to the dry mass, and a $M_C = 66$ % that the wet mass is 1.94 times the dry mass, which is close to the wheat bran moisture saturation. A spore suspension was inoculated into the solid medium by gently mixing it with a volume corresponding to 7.62×10^{-3} g_X/g_{DS} (grams of biomass per grams of dry solid).[16] The incubations were conducted under the operational conditions defined in Table 1 to each column. Runs 1–13, 17, and 18 of the kinetic study were carried out for 72 h, with samples removed at 24 h intervals. All other cultivations were carried out for 42 h.

After the cultivation period, the fermented medium was removed from the column and transferred to a 250 mL Erlenmeyer flask, followed by the addition of 50 mL of sodium acetate buffer (pH 4.8) in order to achieve a solid/liquid ratio of 1:10 (w/v). The suspension was mixed at 200 rpm for 30 min at 32 °C, and the crude enzymatic solution was recovered by filtration followed by centrifugation at 10 000 rpm and 4 °C for 15 min.

Table 1. SSF experimental conditions used for *A. niger* cultivation

Assay	Initial moisture content (M_C)		Temperature (T)	
1	–1	40 %	–1	31 °C
2	–1	40 %	+1	43 °C
3	+1	62 %	–1	31 °C
4	+1	62 %	+1	43 °C
5	–1.4142	36 %	0	37 °C
6	+1.4142	66 %	0	37 °C
7	0	51 %	–1.4142	28 °C
8	0	51 %	+1.4142	46 °C
9	0	51 %	0	37 °C
10	0	51 %	0	37 °C
11	0	51 %	0	37 °C
12*	+0.81	60 %	+0.5	40 °C
13*	+0.81	60 %	–0.5	34 °C
14**	+0.81	60 %	–	variable
15**	+1.41	66 %	–	variable
16**	+1.41	66 %	+0.5	40 °C
17*	+1.41	66 %	–1.1	30 °C
18*	+1.41	66 %	–1.5	27 °C
19***	+1.41	66 %	–	variable
20***	+1.41	66 %	–0.5	34 °C
21***	+1.41	66 %	–0.5	34 °C
22***	+1.41	66 %	–	variable
23***	+1.41	66 %	–	variable

*Model improvement experiments.
**Model validation and process optimization experiments.
***Process optimization experiments.

Respirometric Analysis

Two CO_2 sensors were attached to the bioreactor, both measuring in the range from 0 % to 5 % v_{CO_2}/v_{air}. All growth analyses were based on the CO_2 values. Equation (10) was used in order to transform the volumetric ratio to a molar basis:

$$CO_2 = CO_{2m} F_{air} \rho \frac{1}{MM_{CO_2}} \frac{1}{M_S} \tag{10}$$

where F_{air} is the 1200 mL/h airflow feeding each column; CO_{2m} is the mean of two sampled columns in (v/v); ρ is the CO_2 gas specific mass of 1.801 g/L at 25 °C; MM_{CO_2} is the CO_2 molar mass of 44.1 g/mol, and M_S is the 5 g of dry substrate added to each column.

Determination of Enzyme Activities

The xylanase activity was measured according to the methodology described by Bailey et al.,[21] while endoglucanase was measured following the procedure recommended by Ghose.[22] One unit of activity corresponds to 1 μmol of reducing sugar released per min per mL, under the reaction conditions. Reducing groups were quantified by the dinitrosalicylic acid (DNS) method,[23] with the results expressed as activity units per mass of initial dry solid substrate (U/g).

Experimental Design

A central composite design was used to define a set of eight experiments, plus three central points,[24] within the ranges of temperature and initial moisture content defined in Table 1. Notice that all experiments have been conducted in triplicate. Runs 12, 13, 17, and 18 were carried out to improve the accuracy of the developed model at the specified moisture content, while runs

14–16 and 19–23 were used to evaluate the model improvements and to seek the optimal operational conditions. Cultivation runs 20–23 were conducted over periods of 42 h. Runs 20 and 21 were conducted under static temperature conditions, while runs 22 and 23 employed a temperature profile calculated by the nonlinear integer programming algorithm.

MODEL STRUCTURE

Considering that microbial growth can be described in phases by means of modelling the CO_2 data and regarding the experimental respiration profiles, a three-phase growth model was proposed in this study. This new model is a combination of the models presented in the Theoretical Background section, which has been developed in order to better represent the experimental observations. In all the assays conducted at temperatures below 37 °C and moisture contents above 41 %, a secondary CO_2 peak was observed a few hours after the main peak. Based on this phenomenon, a secondary growth phase, structurally identical to the first phase, but with distinct growth capability, was added to the model. In order to avoid modelling solution errors during the lag phase and accurately represent the initial biomass content adaptation to the medium, the cellular viability factor proposed by Dalsenter et al.[15] was adapted to this model to represent the percentage of cells that are able to grow. Finally, as it was proposed by Dalsenter et al.,[15] the negative effect of temperatures above 32 °C was represented by the cellular inactivation rate coefficient. The new proposed model was written in the form of Equations (11–18).

$$\frac{dF_1}{dt} = \eta F_1(1 - F_1) \tag{11}$$

$$\frac{dF_2}{dt} = \begin{cases} 0, & t < t_a \\ \eta F_2(1 - F_2), & t \geq t_a \end{cases} \tag{12}$$

$$\frac{dX_{a_1}}{dt} = F_1 \mu X_{a_1}\left(1 - \frac{X_{T_1}}{X_{M_1}}\right) - k_d X_{a_1} \tag{13}$$

$$\frac{dX_{T_1}}{dt} = F_1 \mu X_{a_1}\left(1 - \frac{X_{T_1}}{X_{M_1}}\right) \tag{14}$$

$$\frac{dX_{a_2}}{dt} = F_2 \mu X_{a_2}\left(1 - \frac{X_{T_2}}{X_{M_2}}\right) - k_d X_{a_2} \tag{15}$$

$$\frac{dX_{T_2}}{dt} = F_2 \mu X_{a_2}\left(1 - \frac{X_{T_2}}{X_{M_2}}\right) \tag{16}$$

$$r_{CO_2} = Y_{CO_2X}\frac{dX}{dt} + m_{XCO_2}X_a \tag{17}$$

Equations (11) and (12) represent the lag phases for their corresponding growth phases, where $\eta\,(h^{-1})$ is the cellular adaptation rate, which gives the rate that cells become available to grow; and t_a is the time delay for triggering the secondary phase of growth. The subscripts indicate the corresponding growth phases. Equations (13) and (14) describe the viable and total biomasses, respectively, for the primary growth phase, while Equations (15) and (16) provide these parameters for the secondary growth phase. Equation (17) relates the growth and active biomass to the CO_2 produced. In Equation (17), it was assumed that the total grown biomass is represented by $X = X_{T_1} + X_{T_2}$, and the active biomass is represented by $X_a = X_{a_1} + X_{a_2}$, with both, X and X_a, given in grams of biomass per gram of dry substrate,[25] which are respectively describing the CO_2 production rate from cellular maintenance and cellular growth. In addition, it is assumed that Y_{XCO_2} and m_{XCO_2} are independent of variations of operational conditions,[9] while all the parameters of Equations (11–16) are given as a function of the initial moisture content and temperature.[6] The values of Y_{XCO_2} and m_{XCO_2} were estimated as $19.6\,mmol_{CO_2}/g_X$ and $0.98\,mmol_{CO_2}/g_X \cdot h$, respectively, based on data from Sargantanis et al.[26] These values were those that resulted in the best fits of the other parameters for all the operational conditions studied.

The developed growth model was not able to consider the permanent effects of temperature variations above maximum growth on cellular viability. Therefore, a biomass inactivation restriction was added to the model in order to express the way that temperature variations affect the living cells and subsequent growth, as shown in Equation (18). Otherwise, the predicted secondary growth phase would be larger than that observed in a case where, for example, the temperature is increased to 43 °C and then returned to 30 °C. It should be noted that this equation would not have any effect on the model solution if the temperature remained constant during the process.

$$k_d(k) = \max(K_D(k = 0{:}\,t)) \tag{18}$$

In Equation (18), $K_D(k = 0{:}\,t)$ is a time series of the deactivation constant at all past temperature (T) and moisture contents (M_C) recorded at the sample times, e.g. $K_D(t) = k_D(T, M_C, t)$, and $k_D(T, M_C)$ is the polynomial response surface resulting from the fitted parameter interpolation, as described in the next section.

The enzymatic production associated with the growth was described according to the Luedeking-Piret model.[14] Equations (19) and (20) represent the production of the endoglucanase and xylanase enzymes, respectively, where Y_{XEnd} and Y_{XXyl} define their production yields per unit of biomass associated with growth, β_{XEnd} and β_{XXyl} define the product formation rates that are not associated with growth, and $k_{D_{End}}$ and $k_{D_{Xyl}}$ represent the enzyme degradation rates.

$$\frac{dE_{nd}}{dt} = Y_{XEnd}\frac{dX}{dt} + \beta_{XEnd}X - k_{D_{End}}E_{nd} \tag{19}$$

$$\frac{dX_{il}}{dt} = Y_{XXyl}\frac{dX}{dt} + \beta_{XXyl}X - k_{D_{Xyl}}X_{il} \tag{20}$$

All the simulations were performed using Matlab software and the *ode113* variable-order Adams-Bashforth-Moulton solver, since this choice provided a shorter simulation solving time and higher accuracy for the implicit derivative system. In the iterative algorithm, a 1/8 max-step was necessary to prevent model miscalculations, due to the stringent error tolerances when changing the temperature. In addition, this max-step was considered because this model was also developed to be a predictor in a predictive controller, developed in LabVIEW (National Instruments™) to control this process in a larger bioreactor, with temperature sampling time of 15 min.

Parameter Identification and Interpolation Procedures

A "grey-box" identification tool was used to identify the process parameters.[27] The parameters were fitted by the minimization

method, with calculation of the least squares minimization using the Levenberg-Marquardt procedure.[28] Three independent runs of the central point were conducted, with two replicates of CO_2 data acquired to estimate the process standard deviation. For this purpose, the growth parameters were fitted independently for all six measurements and their standard deviations were calculated using Equation (21), which were normalized to all other experimental conditions using Equation (22). Additionally, the products formation confidence intervals were considered a consequence of growth variations, thus, no standard deviation was added to the production parameters. The following procedure shows how the model was developed.

$$\sigma = \sqrt{\frac{1}{N-1}\sum_{i=1}^{6}|P_i - \bar{P}|^2} \tag{21}$$

where P_i represents each calculated parameter value, $\bar{P}$ is the mean, and six is the number of observations.

$$\sigma_N = \sigma/\bar{P} \tag{22}$$

Assuming $\bar{P}_j$ the mean of each parameter calculated at different experimental conditions, then $\sigma_j = \sigma_N \overline{P_j}$ is $\bar{P}_j$ standard deviation.

1st step: Fitting of the growth model, applying Equations (11–17) to the CO_2 data obtained during each of the experimental runs 1–13 (Table 1). Experiments 12 and 13 were performed to improve the modelling accuracy at a moisture content of 60 %.

2nd step: Interpolation of all the growth model parameters (obtained in the 1st step) across the experimental operational conditions, based on a second-degree polynomial surface.

3rd step: Based on the growth model developed in steps 1 and 2, fitting of the enzymatic production kinetics parameters, followed by their interpolations into a second-degree polynomial surface.

4th step: Evaluation of the temperature optimization profiles calculated by the proposed algorithm (experiments 14 and 15) and evaluation of model accuracy (experiment 16).

5th step: Since the experimental enzymatic results at M_C of 60 % were below the values expected for the proposed temperature profiles, experiments 17 and 18 were performed to refine the modelling for temperatures below 37 °C with M_C of 66 %.

6th step: A weighted-parameters interpolation was employed to improve the accuracy of the growth model across the static and variable operational conditions, with M_C greater than 50 %. In the case of the endoglucanase production model, a 3 × 2 degree polynomial (temperature × moisture content) was calculated in order to improve the modelling accuracy at temperatures above 37 °C. This was not necessary for the xylanase modelling.

7th step: Evaluation of a new temperature optimization profile calculated using the proposed algorithm, at M_C of 66 % (experiment 19), followed by a comparison with a fixed temperature profile.

8th step: Some refinements of the weighted parameters interpolation were made in order to improve the CO_2 production rate response under all the operational conditions.

PROCESS OPTIMIZATION

Optimization of Initial Conditions by Mathematical Modelling

Several simulations were carried out to find the optimum temperature and moisture content initial conditions for endoglucanase production. The mathematical model, defined in Equations (11–20), was used with parameters as described in the Parameter interpolation section. The initial moisture content adopted in the simulations was 66 %, since this was the limit that avoided the presence of free water in the medium, with the best production yields. Seventeen simulations were conducted at constant temperature, which varied from 27 °C to 43 °C, with 1 °C intervals. Before the fifth step of subsection Parameter identification and interpolation procedures, the best temperature condition found was 34 °C, which was then evaluated experimentally. After the fifth step, the best proposed operational temperature was 32 °C. The estimated endoglucanase production values, at 42 h fermentation time, were 134 U/g at 34 °C and 140 U/g at 32 °C. Since the difference was not greater than the estimated confidence interval, it was decided that no further experiments would be necessary to validate the modelling.

Iterative Nonlinear Integer Programming Algorithm

The aim of the maximization problem was to identify the temperature profile that would provide the highest endoglucanase production at 42 h after inoculation. An evolutionary search operation was used to iteratively solve a mixed integer nonlinear programming problem,[17] where several paths of discrete temperature variations along the prediction horizon were applied and analyzed at each iteration. After testing all the temperature paths, the first action of the highest production path was recorded, the prediction horizon was moved one step forward, and the search was reinitiated. This procedure was repeated until the process end time was reached.

The objective function of this problem was defined as the maximum endoglucanase production at $t = n + N$, subject to temperature paths p, according to Equation (23). In this problem, a sample step was defined as being 1 h.

$$J = \max_{\mathrm{p}}\left(E_{nd}\left(M_C, T_p, t = n+N\right)\right) \tag{23}$$

subject to:

$$27\,^{\circ}\mathrm{C} < T_p < 43\,^{\circ}\mathrm{C}$$

$$M_C = 66\ \%$$

$$p = \begin{pmatrix} N \\ 3 \end{pmatrix}$$

In Equation (23), n is the current time; N is the prediction horizon in the sample steps; $E_{nd}\left(M_C, T_p, t = n+N\right)$ is the solution of Equation (19), subject to the growth model described by Equations (11–16); and T_p is the process temperature at instant n. The following procedure describes how the iterative algorithm was implemented.

Step 1: Define the initial process temperature (T_u), the initial moisture content (M_C), and the prediction horizon (N). This generates the sequence of actions for the prediction horizon, where $P = \begin{bmatrix} p_1 \\ \vdots \\ p_f \end{bmatrix}$.

Step 2: For $n = 0\ to\ 42$; $T_p(n) = T_u$.

Step 2.1: For $i = 1\ to\ f$; Simulate Equations from (11) to (20) at medium temperature $T_m = \begin{cases} T_p(t), & t < n \\ T_p(n) + p_i, & t \geq n \end{cases}$; $f = f + 1$;

$End_p(i) = E_{nd}(M_C, T_p, t = n + N)$; where t is the internal ordinary differential equation solver time counter; end for.

Step 3: $[J, position] = \max_p(End_p)$; $T_u = T_p(n) + p(1, position)$; $n = n + 1$; *if* $n < 42$ then return to Step 2, else end for.

Step 4: Return T_p, $E_{nd}(t = 42)$; end procedure.

After the fifth step of the modelling, a different objective function was tried. For example, instead of searching for the maximum endoglucanase productivity at the end of the prediction horizon, its final temperature condition was maintained until the end of the 42 h proposed here. In this last search, the iterative algorithm returned that a constant 32 °C temperature for the process would return the maximum production. However, as noted previously, since the improvements were small, it was considered that no further tests would be necessary.

RESULTS AND DISCUSSION

Secondary CO_2 peaks were observed later in the process in runs 3, 7, 17, and 18, as illustrated in Figure 1a. These peaks were more pronounced in the experiments performed at temperatures below 31 °C and initial moisture contents above 51 %, and were also noted at 37 °C and 51 % moisture content, as shown in Figure 1b, but were less apparent than under the former conditions. Four independent experiments were conducted in the central point and, in three of them, the CO_2 data was measured from two replicate columns, as presented in Figure 1b. Distinct respiratory profiles were obtained at this operational condition. Concerning the modelling, it shows that the specific growth rate, the maximum biomass concentration, and the death constant varied among the experiments. The specific growth rate is related to the CO_2 ascent slope, the maximum biomass per mass of dry substrate is related to the respiration amplitude, and the inactivation constant to descent slope observed after the peak.

The temporal profiles of xylanase and endoglucanase production are shown in Table 2. Product formation differed among assays performed under the same operational conditions, with endoglucanase production showing greater between-batch variability than xylanase production. Under all operational conditions, for xylanase production the highest values were recorded at either 24 h and 48 h, while the endoglucanase peak occurred at 48 h. Both enzymes' production rates were faster at higher temperature (40 °C) and moisture content (66 %), although the highest yields, among all tested conditions, were obtained after 48 h at 30 °C and 66 % moisture content. At 46 °C, no growth was detected and there was almost no enzyme production.

Estimation of Growth and Production Kinetic Parameters

The results of fitting of the growth model parameters are shown in Table 3, with kinetics shown in the figure presented in the supplementary material. These parameters were calculated as described in Equations (21–22). Since no growth was observed in experimental run 8, and product formation was 20-fold lower than for the central point, these data were not taken into consideration. The maximum specific growth and the maximum biomass concentrations were close to those reported in the literature, respectively between 0.17 h^{-1} and 0.27 h^{-1} and from 0.15 g_X/g_{DM} to 0.34 g_X/g_{DM}, for *Aspergillus niger* cultivated in wheat bran, under temperature conditions varying from 30 to 40 °C and moisture content from 45 to 65 % (w/w).[5,9] No data was found for the deactivation constant for *A. niger* used in a similar manner as the modelling proposed here. Concerning the lag phase, it is usually fitted by adjusting the initial biomass value, irrespective of the amount inoculated in the process.[5,11] Conversely, the amplitude of η is what determines the rate that the inoculated biomass begins to grow.

By calculating a second-degree polynomial response surface of Table 2 parameter data (data not shown), μ and X_{M_1} present their highest values around 34 °C at 66 % M_C. A similar behaviour was observed for k_d, while the maximum values of η stay at 37 °C and 51 % M_C. This indicates that the maximum respiration rates are found close to 37 °C and 66 % M_C. Continuing this analysis, the secondary CO_2 peak, which is directly dependent on X_{M_2}, becomes more pronounced at 34 °C and 55 % M_C, indicating that the fungus latter growth is higher around this operating condition.

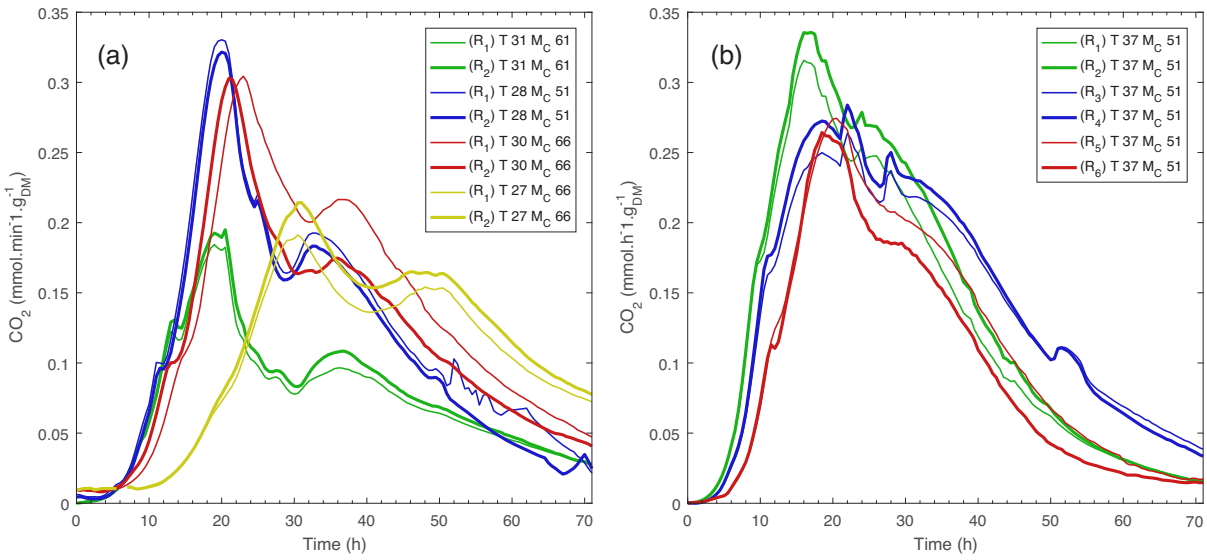

Figure 1. Measured CO_2 production at different operational conditions during SSF cultivation of *A. niger*: (a) microbial growth evolution and reproduction variability under the different moisture content conditions and temperature below 31 °C, (b) microbial growth evolution reproducibility under the same operational conditions, 51 % M_C, and 37 °C. R_i refers to the experimental replication number.

Table 2. Endoglucanase and xylanase production kinetics and production at 42 h

Assays			Xylanase (U/g_{DM})			Endoglucanase (U/g_{DM})		
	T (°C)	M_C (%)	24 h	48 h	72 h	24 h	48 h	72 h
R1	37	51	142 ± 2	155 ± 5	140 ± 4	34.0 ± 4.6	47.4 ± 1.3	45.3 ± 2.5
R2	37	51	146 ± 5	168 ± 6	115 ± 11	44.5 ± 4.0	75.7 ± 1.1	72.8 ± 4.8
R3	37	51	157 ± 3	136 ± 5	152 ± 12	40.6 ± 1.8	71.0 ± 0.5	67.7 ± 1.9
R4	37	51	70 ± 7	75 ± 4	60 ± 1	39.1 ± 1.3	45.1 ± 1.1	72.8 ± 8.3
1	31	40	158 ± 7	157 ± 6	140 ± 16	26.4 ± 2.9	43.4 ± 4.9	36.8 ± 0.4
2	43	40	87 ± 5	174 ± 9	109 ± 6	15.0 ± 2.4	38.9 ± 1.9	35.9 ± 2.5
3	31	61	121 ± 9	181 ± 1	153 ± 5	19.9 ± 4.6	63.7 ± 2.3	37.2 ± 3.5
4	43	61	119 ± 14	199 ± 5	202 ± 5	28.6 ± 3.4	65.3 ± 1.0	74.6 ± 6.2
5	37	36	131 ± 18	121 ± 11	94 ± 9	46.3 ± 1.5	51.0 ± 0.5	50.8 ± 3.7
6	37	66	171 ± 6	171 ± 5	116 ± 4	39.8 ± 2.1	63.8 ± 1.5	78.9 ± 1.0
7	28	51	101 ± 3	154 ± 11	143 ± 4	18.2 ± 1.0	75.9 ± 4.0	67.7 ± 4.4
8	46	51	4.6 ± 0.3	4.4 ± 0.5	3.7 ± 0.7	4.0 ± 0.4	4.8 ± 1.6	3.3 ± 1.6
12	40	60	172 ± 11	204 ± 3	155 ± 2	64.7 ± 7.6	76.6 ± 23.3	74.8 ± 1.5
13	34	60	148 ± 3	165 ± 7	127 ± 5	50.1 ± 5.4	74.3 ± 6.5	70.3 ± 2.2
17	30	66	123 ± 6	274 ± 22	252 ± 3	36.7 ± 2.7	160.2 ± 21.1	149.6 ± 17.7
18	27	66	87 ± 9	229 ± 9	248 ± 4	37.8 ± 5.4	101.3 ± 14.1	156.6 ± 16.4
			42 h			42 h		
14	P1	60	190 ± 3			69 ± 12		
15	P2	66	181 ± 26			123 ± 12		
16	40	66	239 ± 1			91 ± 5		
19	P3	66	226 ± 5			132 ± 9		
20/21	34	66	188 ± 38			96 ± 35		
22/23	P4	66	170 ± 7			90 ± 8		

Despite the considerations about fungal growth, the enzymatic production strongly depends on the product formation pathways, which are related to the process conditions. The results of the fitted product formation, presented in Table 4, were based on the interpolated growth parameters, as shown in the Parameters Interpolation subsection. According to Table 4 data, by increasing the temperature, the endoglucanase production moves from non-growth-associated to growth-associated. The xylanase production was predominantly growth-associated, in spite of that, the lower the temperature, the higher the non-growth-associated production yield. Here, the response surface observations cannot be directly conducted as they were for biomass growth parameters, because the enzymatic production also depends on the biomass concentration. Thus, despite the highest xylanase production yield having been estimated at a temperature below 30 °C and 40 % M_C, the highest production, according to Table 2, was measured at 30 °C and 66 % M_C at 48 h. At these latter operating conditions, the non-growth-associated product formation is more relevant than at the former.

The endoglucanase production was more sensitive to temperature variations. As shown in Table 4, the growth associated production yields vary from zero, at 28 °C, to 556 $\left(U_{Xil} \cdot g_X^{-1} \cdot g_{DS}^{-1}\right)$, at 37 °C. On the other hand, the non-growth associated production yields are the opposite, changing from zero at 40 °C to 82 at 30 °C. Again, the maximum production was measured at 30 °C, showing the importance of the non-growth associated pathway for these enzyme productions. Both enzymes showed the highest degradation rates at lower temperatures, around 51 % M_C for

Table 3. Calculated growth model parameters for each experimental condition

Assays			lag_2	μ	k_d	X_{M_1}	X_{M_2}	
T (°C)	M_C (%)	η	(h)	(h^{-1})	(h^{-1})	(g_X/g_{DM})	(g_X/g_{DM})	R^2
31	40	0.98 ± 0.02	25.4 ± 2.4	0.19 ± 0.02	0.02 ± 0.01	0.11 ± 0.01	0.02 ± 0.00	0.90
43	40	0.76 ± 0.02	17.3 ± 1.5	0.20 ± 0.02	0.03 ± 0.01	0.12 ± 0.01	0.00 ± 0.00	0.91
31	61	0.98 ± 0.02	20.4 ± 2.0	0.33 ± 0.04	0.04 ± 0.01	0.15 ± 0.01	0.04 ± 0.00	0.86
43	61	0.94 ± 0.02	18.1 ± 1.7	0.24 ± 0.03	0.02 ± 0.01	0.20 ± 0.01	0.03 ± 0.00	0.91
37	36	1.14 ± 0.02	18.0 ± 1.7	0.35 ± 0.04	0.06 ± 0.01	0.12 ± 0.01	0.04 ± 0.00	0.92
37	66	1.15 ± 0.02	20.1 ± 2.0	0.33 ± 0.04	0.06 ± 0.01	0.20 ± 0.01	0.05 ± 0.01	0.91
31	40	1.30 ± 0.02	24.6 ± 2.4	0.27 ± 0.03	0.03 ± 0.01	0.09 ± 0.01	0.02 ± 0.00	0.80
28	51	1.09 ± 0.02	24.4 ± 1.9	0.33 ± 0.03	0.05 ± 0.01	0.18 ± 0.01	0.06 ± 0.01	0.91
37	51	1.77 ± 0.02	22.5 ± 2.4	0.30 ± 0.03	0.03 ± 0.01	0.09 ± 0.01	0.02 ± 0.00	0.88
40	60	1.42 ± 0.02	22.5 ± 1.8	0.28 ± 0.04	0.04 ± 0.01	0.14 ± 0.02	0.04 ± 0.01	0.88
34	60	1.30 ± 0.02	17.7 ± 0.8	0.34 ± 0.04	0.06 ± 0.01	0.22 ± 0.01	0.06 ± 0.00	0.95
30	66	0.85 ± 0.02	21.3 ± 2.1	0.30 ± 0.03	0.04 ± 0.01	0.15 ± 0.01	0.05 ± 0.00	0.90
27	66	0.67 ± 0.02	26.2 ± 2.5	0.22 ± 0.03	0.03 ± 0.01	0.12 ± 0.01	0.04 ± 0.00	0.90

Table 4. Product formation modelling parameters for each experimental condition

T (°C)	M_C (%)	Y_{XEnd}	β_{XEnd}	$k_{D_{End}}$	R^2_{End}	Y_{XXyl}	β_{XXyl}	$k_{D_{Xyl}}$	R^2_{Xyl}
37	51	32.0	39.0	0.036	0.96	1128.3	0.00	0.013	0.99
37	36	555.9	0.03	0.010	0.96	1833.7	0.15	0.025	0.99
37	66	197.6	7.04	0.000	0.90	1287.8	0.08	0.020	0.99
28	51	0.00	50.0	0.055	0.87	1374.4	12.4	0.015	0.98
31	40	5.50	45.0	0.053	0.94	1874.8	0.25	0.014	0.99
43	40	318.6	5.75	0.020	0.99	2274.3	22.1	0.041	0.99
31	62	0.00	29.4	0.020	0.94	1118.7	0.03	0.003	0.98
43	62	281.3	2.97	0.000	0.94	1243.9	0.08	0.005	0.99
40	60	456.9	0.00	0.007	0.90	1357.1	0.01	0.014	0.99
34	60	251.1	15.1	0.007	0.95	1114.3	0.01	0.014	0.95
30	66	0.00	82.2	0.028	0.92	713.10	129.4	0.037	0.99
27	66	0.00	75.7	0.029	0.88	1145.4	180.0	0.061	0.89

endoglucanase and, in the case of xylanase, at higher moisture contents.

Parameter interpolation

In the weighted interpolation, as shown in Equations (24–29), the fits of the parameters were relatively low: $R^2_{\mu} = 81\ \%$; $R^2_{k_d} = 63\ \%$; $R^2_{X_{M_1}} = 65\ \%$; $R^2_{X_{M_2}} = 69\ \%$; $R^2_{\eta} = 87\ \%$; $R^2_{lag_2} = 63\ \%$. However, it is important to note that the objective of this approach did not concern the individual parameter fits, but rather a satisfactory representation of the experimental observations at moisture content close to 66 %. In this sense, at 66 % M_C, the R^2 for the experiments at the temperatures of 27, 30, 37, and 40 °C were, respectively, 89, 88, 90, and 94 %, while for the experiments at 31, 34, 40, and 43 °C, under 60 % M_C, the R^2 were, respectively, 83, 77, 85, and 64 %. At 51 % of MC and 37 °C the R^2 was 87 %. In addition, the modelling was developed to represent the process confidence interval, so some variations in the growth profiles were expected.

$$\mu(M_C,T) = -1.358 - 10.5\,10^{-3}M_C + 0.108T + 7.29\,10^{-5}M_C{}^2 - 1.63\,10^{-3}T^2 + 1.32\,10^{-4}M_CT \quad (24)$$

$$k_d(M_C,T) = -0.822 + 3.69\,10^{-3}M_C + 0.043T + 3.35\,10^{-6}M_C{}^2 - 5.2\,10^{-4}T^2 - 5.24\,10^{-4}M_CT \quad (25)$$

$$\eta(M_C,T) = -11.6 + 0.198M_C + 0.441T - 1.96\,10^{-4}M_C{}^2 - 6.16\,10^{-3}T^2 + 1.53\,10^{-4}M_CT \quad (26)$$

$$lag_2(M_C,T) = -37.55 + 2.96M_C - 0.491T - 19.1\,10^{-3}M_C{}^2 - 0.029T^2 + 22.4\,10^{-3}M_CT \quad (27)$$

$$X_{M_1}(M_C,T) = -1.36 + 0.018M_C + 0.053T - 1.27\,10^{-4}M_C{}^2 - 6.4\,10^{-4}T^2 - 8.6\,10^{-5}M_CT \quad (28)$$

$$X_{M_2}(M_C,T) = -0.97 + 0.013U + 0.038T - 7.77\,10^{-5}M_C{}^2 - 4.52\,10^{-4}T^2 - 1.3\,10^{-4}M_CT \quad (29)$$

For xylanase production, a second-degree polynomial interpolation presented the necessary accuracy to describe the kinetics under all the required conditions. In the case of endoglucanase, a third-degree polynomial for temperature and a second-degree polynomial for moisture content were required in order to obtain a better description of the kinetics. A weighting procedure was also tested, but the best results were achieved using an unweighted interpolation. Equations (30–35) describe the fitted surfaces, where the accuracies of the fits for the enzymatic production were: $R^2_{Y_{XEnd}} = 57\ \%$; $R^2_{\beta_{XEnd}} = 89\ \%$; $R^2_{k_{D_{End}}} = 89\ \%$; $R^2_{Y_{XXyl}} = 83\ \%$; $R^2_{\beta_{XXyl}} = 82\ \%$; $R^2_{k_{D_{Xyl}}} = 82\ \%$.

$$Y_{XEnd}(M_C,T) = -5.31\,10^4 + 1465M_C + 2335T - 9.56M_C{}^2 - 21.58T^2 - 56.79M_CT + 0.29M_C{}^2T + 0.36M_CT^2 + 7.48\,10^{-3}T^3 \quad (30)$$

$$\beta_{XEnd}(M_C,T) = 4880 - 257.3M_C - 4.25T + 1.95M_C{}^2 - 6.71T^2 + 8.51M_CT - 0.041M_CT^2 - 0.053M_C{}^2T + 0.087T^3 \quad (31)$$

$$k_{D_{End}}(M_C,T) = 3.03 - 0.080M_C - 0.124\mathrm{T} + 4.63\,10^{-4}M_C{}^2 + 7.7\,10^{-4}T^2 - 3.2\,10^{-4}M_CT - 1.52\,10^{-5}M_C{}^2T - 2.20\,10^{-5}M_CT^2 + 5.82\,10^{-6}T^3 \quad (32)$$

$$Y_{XXyl}(M_C,T) = 10430 - 126.0M_C - 308.1T + 0.819M_C{}^2 + 4.46T^2 + 0.261M_CT \quad (33)$$

$$\beta_{XXyl}(M_C,T) = 820.4 - 6.10M_C - 38.59T + 0.22M_C{}^2 + 0.805T^2 - 0.412M_CT \quad (34)$$

$$k_{DXXyl}(M_C,T) = 0.127 - 9.98\,10^{-4}M_C - 5.23\,10^{-3}T + 6.91\,10^{-5}M_C{}^2 + 2.03\,10^{-4}T^2 - 1.76\,10^{-4}M_CT \quad (35)$$

A cardinal temperature model with inflection was used by Saithi et al.[12] to estimate growth and enzymatic production process parameters. Despite achieving reasonable accuracy for temperature, estimates of moisture content were not feasible. Mitchell et al.[6] suggested the use of a fourth-order polynomial to estimate some model parameters, which was used by Casciatori et al.[29] Nevertheless, the large number of experiments required would be excessive. Considering the results presented here, the present technique is a simpler option capable of representing the process, within the range of operational conditions considered.

Growth and Enzymatic Production Kinetics

Figure 2 shows the experimental endoglucanase, xylanase, and cellular respiration profiles, together with the model estimates, for a moisture content of 66 % and constant temperatures of 40, 37, 34, 30, and 27 °C. Figures 2a–e show the results for endoglucanase, Figures 2f–j show the xylanase results, and Figures 2h–o illustrate the corresponding respiratory profiles. The estimations were carried out by running 1000 simulations with randomly generated parameters, restricted to the confidence intervals and with normal distributions. The coloured graphs are the simulated observation histograms with 1 h sampling intervals, where red indicates a higher probability of occurrence, dark green indicates the 90 % confidence interval, and light green indicates the 95 % confidence interval. It should be noted that at $t = 0$ h, the number of observations was equal to the number of simulations. The red level was obtained by measuring the maximum number of observations at $t = 42$ h, in order to balance the colour map, with dark red indicating a number of observations greater than 90. The graphs indicate the frequency at which an event occurred, but do not show the profile generated to achieve a certain value. It should be noted that production variability is an inherent feature of biological processes. As examples, a variation of 12.5 % was observed between duplicates in the case of protease production,[30] while a ±20 % variation was found for endoglucanase production.[31]

All the experimental respiration profiles were within the confidence intervals (Figure 2), but this was not the case for all the enzymatic production profiles, as observed in the 40 °C endoglucanase production (Figure 2a). For this experiment, the mean of the simulated data was only within a 99 % confidence interval, being statistically different for this analysis. However, it is important to consider that a variation of ±20 % in endoglucanase production is not uncommon.[31] All other enzymatic production data were within a 95 % confidence interval, despite some outliers, based on the *t*-student distribution. The run at 34 °C was executed twice in order to evaluate the process confidence intervals under both modelled and non-modelled conditions (Figures 2c, 2h, and 2m). A comparison of the enzymatic production with the growth kinetics showed that the latter was more reliable, under the evaluated experimental conditions.

The respiration profiles in Figure 2 show that as the temperature increased, the CO_2 production rates increased, together with the maximum CO_2 produced. On the other hand, the secondary respiration peak increased as the temperature decreased, resulting in the production of greater amounts of CO_2 at the end of the fermentation.

In addition, the maximum enzymatic production yields were found between 30 and 34 °C. In this temperature range, the endoglucanase production parameters moved from non-growth-associated to growth-associated and the maximum secondary growth yields occurred. For xylanase, in all evaluated conditions, the fungus produced it mainly in the growth-associated pathway. However, for temperatures below 30 °C under 66 % M_C, the non-growth-associated production parameter appeared more pronounced.

As the temperature was raised above 34 °C, xylanase ceased to be produced according to a non-growth-associated mechanism. For the A. niger cultivated in wheat bran, under 55 % M_C in wet

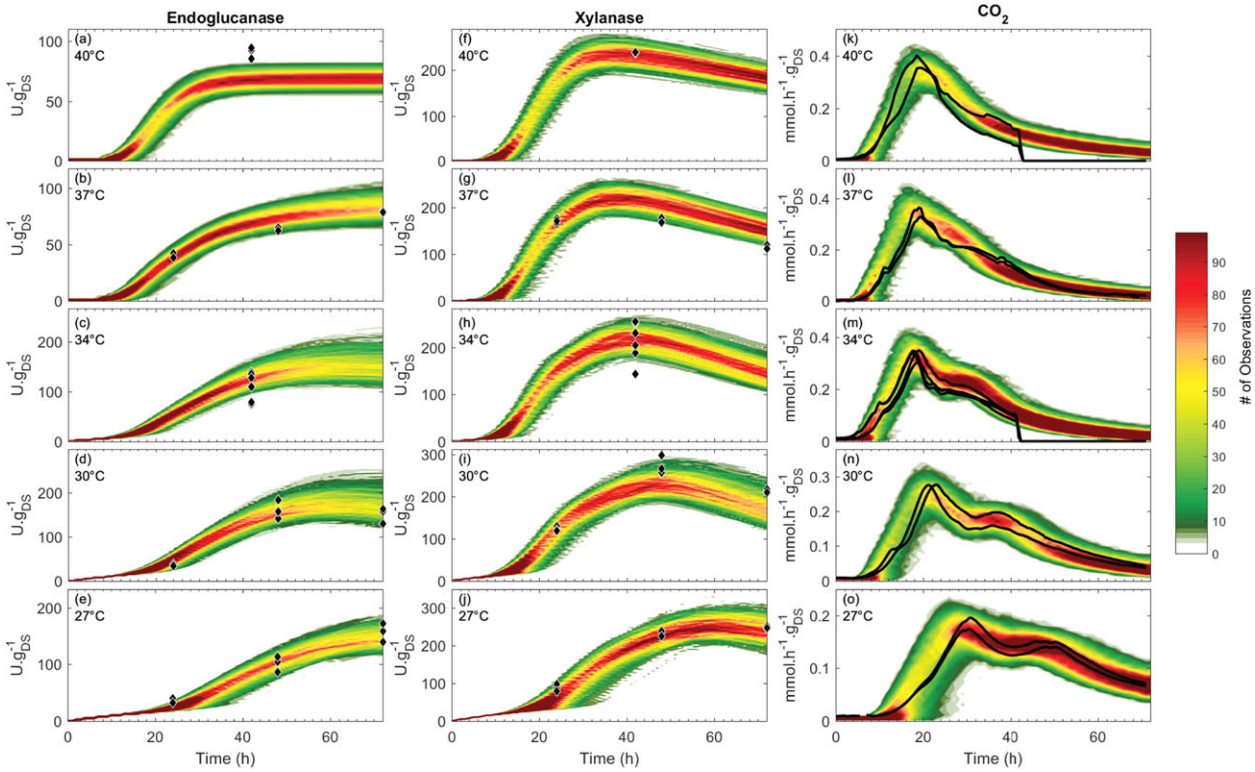

Figure 2. Estimated and measured endoglucanase, xylanase, and CO_2 production kinetics at different temperatures: (a), (b), (c), (d), and (e) show endoglucanase production at 40, 37, 34, 30, and 27 °C, respectively; (f), (g), (h), (i), and (j) show the corresponding xylanase production; (k), (l), (m), (n), and (o) show the corresponding CO_2 production. The black diamonds are the experimental enzymatic results and the black lines are the observed CO_2 profiles.

weight, Hamidi-Esfahani et al.[9] found that the maximum O_2 uptake rate peak, which is closely related to the maximum growth (X_M), occurred at temperatures above 34 °C. In addition, the steepest oxygen uptake rate, which is more closely related to the specific growth rate parameter (μ) than the maximum growth, occurred between 30 and 34 °C. The growth model parameters calculated in Table 3 are in accordance with these observations.

Temperature Effects and Modelling Improvements

The temperature profiles are shown in Figure 3, together with the experimental results. Profiles P1, P2, and P3 (Figures 3a, 3e, and 3i) correspond to assays 15, 19, and 22 (Table 1), respectively. Figures 3b–d show the experimental data and the simulated results for endoglucanase, xylanase, and CO_2 production, respectively, for profile P1. Figures 3f–h show the experimental and estimated results for profile P2, and Figures 3j–l show the results for profile P3. It can be seen from these results that the model provided accurate representations of the fermentations. The third profile was carried out twice in order to validate the estimated confidence interval. Here, both the xylanase and the respiration profiles stayed at the 95 % confidence interval bounds, but not the endoglucanase. This reinforces the literature findings,[31] since endoglucanase production is more sensitive to environmental and process conditions than the xylanase enzymes. These fermentations were conducted during 42 h.

For both P2 and P3, the use of Equation (18) had almost no effect on the observed or estimated CO_2 data. This could be explained by the fact that for most of the time, in both profiles, the temperature remained around the maximum calculated values of k_D, so the model was not sensitive to such variations. However, there was a significant effect in the case of P1, where the second growth phase CO_2 levels would have been the same as in the first phase, if the equation had not been used (data not shown). Hence, use of this modelling restriction helped in describing how the temperature affected fungal growth at any time of the process. Compared with the restriction used by Dalsenter et al.,[15] this showed that both approaches achieved their objectives concerning the health of cells when exposed to higher temperatures. However, in the present case, a more complex set of equations was employed to describe growth rates, and the effects of temperature on enzymatic production were also determined. In addition, the respiration rate approach provided more information about the process, compared to the accumulated biomass/respiratory approach.

In an investigation of the effects of temperature variations on *Rhizopus oligosporus*, Ikasari et al.[10] found that temperature increases forced the fungus to adapt in order to produce heat-stable proteins and enzymes, replacing those that were lost during the exposure to high temperatures. Consequently, growth would slow during adaptation to temperature upshifts and downshifts, since the adaptations consumed energy. This helps in understanding why the three experimental CO_2 profiles showed small delays, compared with the estimated profiles, despite presenting the expected shapes.

Process Optimization

After calculating the third profile, some minor adjustments were required in the parameter interpolations, which were performed in the fifth step of the model development. Before this step, P3 was

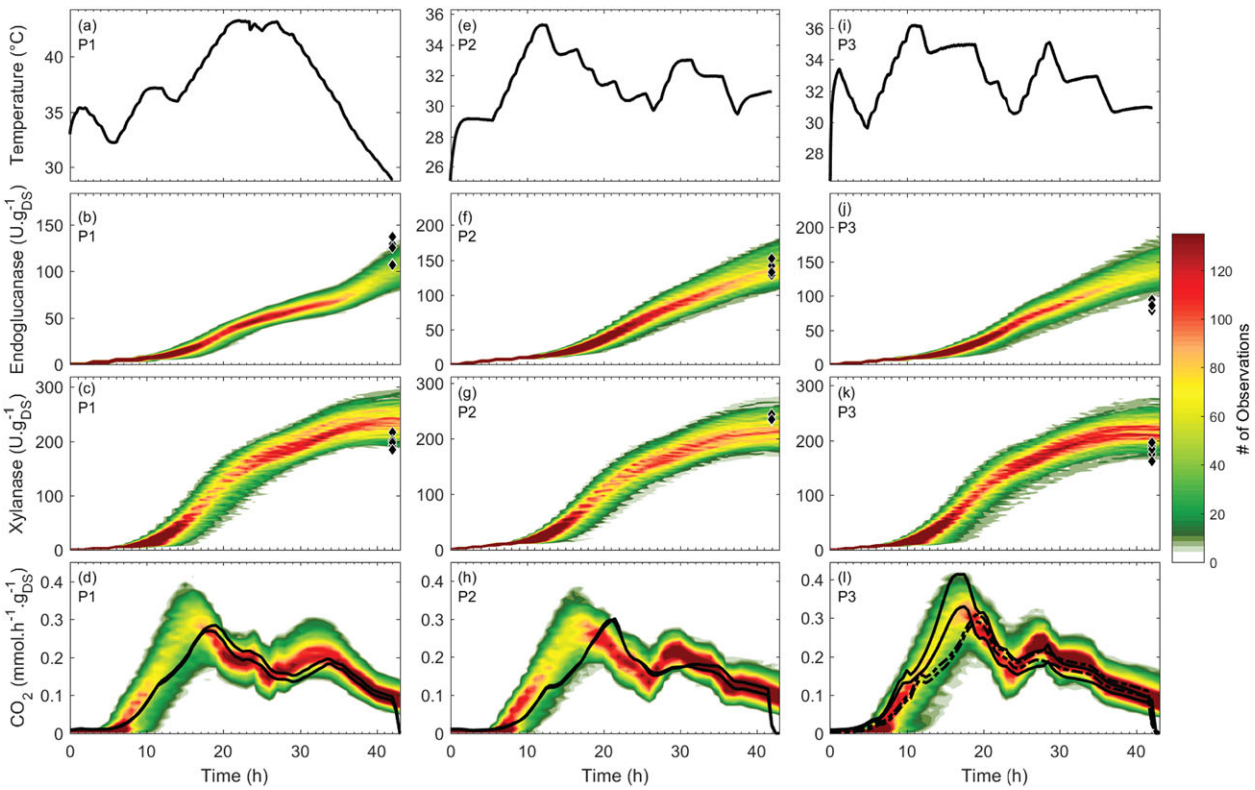

Figure 3. Effects of temperature variation on enzymatic production and respiratory kinetics: (a), (e), and (i) show the temperature profiles used (P1, P2, and P3); (b), (f), and (j) show the estimated endoglucanase formation kinetics and the experimental data at 42 h; (c), (g), and (k) show the estimated xylanase formation kinetics and the experimental data at 42 h; (d), (h), and (l) show the estimated respiration kinetics and the experimental data during the 42 h process. The black diamonds are the experimental enzymatic results and the black lines are the experimental CO_2 profiles.

the temperature profile that should maximize endoglucanase production. However, after updating the modelling with the new parameter interpolation functions, it was found that a profile very similar to that of P2 would improve production yields. In addition, it was found that the best endoglucanase results would be obtained at a constant temperature of 32 °C, with a value (138.5 U/g) very close to the estimated value obtained in P2 (139.1 U/g). These values were two-fold higher than obtained for the central point in the 48 h process (60.0 U/g at 37 °C and 51 % moisture content).

An important consideration is that in the presence of temperature fluctuations, the fungus must adapt to produce enzymes that are less thermolabile.[10] Therefore, given that the best sugarcane enzymatic hydrolysis occurs at 50 °C, and can take up to 72 h,[32] it is possible that enzymes produced under varying conditions might be more efficient in such a long-term process.

The aim of the process optimization developed here was to achieve higher yields of endoglucanase in a faster batch process, saving time that could be used in downstream operations, bioreactor cleaning, and process re-initiation. In a 48 h fermentation cycle, 6 h should be dedicated to these activities, so the process itself should have a duration of 42 h. According to the estimations, the enzymatic production of a process conducted for 48 h at 32 °C would not be significantly greater than at 42 h. However, the cycle would have a duration of 54 h, with consequent negative economic and human resource impacts.

CONCLUSIONS

The proposed model provided accurate predictions of the experimental observations for both enzymatic production and respiratory kinetic profiles during fungal cultivation in SSF under different temperature conditions. A wide range of initial moisture contents were evaluated, with the model indicating the best results at 66 % M_C, due to the influence of the weighted parameter interpolation procedure. The restriction used helped in estimating the effects of high temperature variations, resulting in better process prediction. The iterative mixed integer nonlinear programming algorithm achieved the objective of estimating the varying temperature conditions along the process that maximize endoglucanase production, when compared to the best static one. Furthermore, the use of the proposed set of equations enabled estimation of both the viable and total biomass in the process, which implies that this model can be used to describe the heat generated by fungal growth and maintenance. These findings demonstrate that this model can be useful for optimizing larger-scale SSF processes.

ACKNOWLEDGEMENTS

The authors thank the Brazilian agencies Fapesp, Capes, CNPq, and Embrapa Instrumentation for financial support, and the staff of Embrapa Instrumentation for technical assistance.

NOMENCLATURE

μ	specific growth rate (h^{-1})
$X_{M_{1,2}}$	maximum biomass per gram of dry substrate by growth phase g_X/g_{DS}
k_d	cellular inactivation rate (h^{-1})
$X_{a_{1,2}}$	active biomass by growth phase g_X
$X_{T_{1,2}}$	total biomass by growth phase g_X
η	specific cellular adaptation rate to the medium (h^{-1})
t_a	second growth phase starting time (h)
Y_{XEnd}	associated to growth endoglucanase formation yield per gram of dry substrate $\frac{U_{End}}{g_X g_{DS}}$
m_{End}	non-associated to growth endoglucanase formation yield per gram of dry substrate $\frac{U_{End}}{g_X g_{DS} h}$
Y_{XXil}	associated to growth xylanase formation yield per gram of dry substrate $\frac{U_{Xil}}{g_X g_{DS}}$
m_{Xil}	non-associated to growth xylanase formation yield per gram of dry substrate $\frac{U_{Xil}}{g_X g_{DS} h}$
$k_{D_{End}}$	endoglucanase degradation rate per gram of dry substrate $\frac{U_{End}}{g_{DS} h}$
$k_{D_{Xyl}}$	xylanase degradation rate per gram of dry substrate $\frac{U_{Xil}}{g_{DS} h}$
$\frac{dX_{a_{1,2}}}{dt}$	active biomass growth rate per gram of dry substrate by growth phase $\frac{g_X}{g_{DS} h}$
$\frac{dX_{T_{1,2}}}{dt}$	total biomass growth rate per gram of dry substrate by growth phase $\frac{g_X}{g_{DS} h}$
$\frac{dF_{1,2}}{dt}$	cellular adaptation rate to the solid medium by growth phase (h^{-1})
$\frac{dE_{nd}}{dt}$	endoglucanase production rate per gram of dry substrate $\frac{U_{End}}{g_{DS} h}$
$\frac{dX_{il}}{dt}$	xylanase production rate per gram of dry substrate $\frac{U_{Xil}}{g_{DS} h}$
r_{CO_2}	CO_2 production rate per gram of dry substrate $\frac{mmol}{g_{DS} h}$

REFERENCES

[1] E. Gasiorek, *Chem. Pap.* **2008**, *62*, 141.

[2] M. El-Bakry, J. Abraham, A. Cerda, R. Barrena, S. Ponsa, T. Gea, A. Sanchez, *Crit. Rev. Env. Sci. Tec.* **2015**, *45*, 1999.

[3] C. S. Farinas, *Renew. Sust. Energ. Rev.* **2015**, *52*, 179.

[4] H. A. Ruiz, R. M. Rodriguez-Jasso, R. Rodriguez, J. C. Contreras-Esquivel, C. N. Aguilar, *Biochem. Eng. J.* **2012**, *65*, 90.

[5] Z. Hamidi-Esfahani, S. Shojaosadati, A. Rinzema, *Biochem. Eng. J.* **2004**, *21*, 265.

[6] D. A. Mitchell, N. Krieger, M. Berovic, *Solid-State Fermentation Bioreactors*, Springer-Verlag, London **2006**.

[7] F. J. Weber, J. Tramper, A. Rinzema, *Biotechnol. Bioeng.* **1999**, *65*, 447.

[8] D. M. Stuart, D. A. Mitchell, *J. Chem. Technol. Biot.* **2003**, *78*, 1180.

[9] Z. Hamidi-Esfahani, P. Hejszi, S. A. Shojaosadati, M. Hoogschagen, E. Vasheghani-Farahani, A. Rinzema, *Biochem. Eng. J.* **2007**, *36*, 100.

[10] L. Ikasari, D. A. Mitchell, D. M. Stuart, *Biotechnol. Bioeng.* **1999**, *64*, 722.

[11] L. Ikasari, D. A. Mitchell, *Biotechnol. Bioeng.* **2000**, *68*, 619.

[12] S. Saithi, J. Borg, M. Nopharatana, A. Tongta, *Journal of Microbial & Biochemical Technology* **2016**, *8*, 123.

[13] M. J. Carlile, S. C. Watkinson, G. W. Gooday, *The Fungi*, Academic Press, London **2001**.

[14] M. L. Shuler, F. Kargi, *Bioprocess Engineering: Basic Concepts*, Prentice Hall, Upper Saddle River **2002**.

[15] F. Dalsenter, G. Viccini, M. Barga, D. Mitchell, N. Krieger, *Process Biochem.* **2005**, *40*, 801.

[16] C. S. Farinas, G. L. Vitcosque, R. F. Fonseca, V. B. Neto, S. Couri, *Ind. Crop. Prod.* **2011**, *34*, 1186.

[17] L. Costa, P. Oliveira, *Comput. Chem. Eng.* **2001**, *25*, 257.
[18] A. B. Diaz, A. Blandino, C. Webb, I. Caro, *Appl. Microbiol. Biot.* **2016**, *100*, 9555.
[19] M. Raimbault, D. Alazard, *Eur. J. Appl. Microbiol. Biot.* **1980**, *9*, 199.
[20] O. F. von Meien, L. F. L. Luz, D. A. Mitchell, J. R. Perez-Correa, E. Agosin, M. Fernandez-Fernandez, J. A. Arcas, *Chem. Eng. Sci.* **2004**, *59*, 4493.
[21] M. J. Bailey, P. Biely, K. Poutanen, *J. Biotechnol.* **1992**, *23*, 257.
[22] T. K. Ghose, *Pure Appl. Chem.* **1987**, *59*, 257.
[23] A. Berlin, V. Maximenko, N. Gilkes, J. Saddler, *Biotechnol. Bioeng.* **2007**, *97*, 287.
[24] B. Singh, R. Kumar, N. Ahuja, *Crit. Rev. Ther. Drug* **2005**, *22*, 27.
[25] J. Liu, D. B. Li, J. C. Yang, *Appl. Biochem. Micro.+* **2007**, *43*, 211.
[26] J. Sargantanis, M. N. Karim, V. G. Murphy, D. Ryoo, R. P. Tengerdy, *Biotechnol. Bioeng.* **1993**, *42*, 149.
[27] T. P. Bohlin, *Practical grey-box process indentification: theory and applications*, 1st edition, Springer-Verlag, London **2006**, p. 351.
[28] L. Thomas, C. Larroche, A. Pandey, *Biochem. Eng. J.* **2013**, *81*, 146.
[29] F. P. Casciatori, A. Bueck, J. C. Thomeo, E. Tsotsas, *Chem. Eng. J.* **2016**, *287*, 103.
[30] R. Banerjee, B. C. Bhattacharyya, *Biochem. Eng. J.* **2003**, *13*, 149.
[31] R. D. P. B. Pirota, L. S. Miotto, P. S. Delabona, C. S. Farinas, *Braz. J. Chem. Eng.* **2013**, *30*, 117.
[32] V. M. Vasconcellos, P. W. Tardioli, R. L. C. Giordano, C. S. Farinas, *New Biotechnol.* **2016**, *33*, 331.

Manuscript received July 5, 2017; revised manuscript received September 20, 2017; accepted for publication October 26, 2017.